Dynamic Focal Spot Size Using a Static Phase Plate

Colin James Parker, Brighton High School

1. ABSTRACT

A distributed phase plate (DPP) is designed for the University of Rochester Laboratory for Laser Energetics OMEGA laser system that can manipulate the focal spot size during a three-nanosecond pulse. These hybrid full aperture diffractive elements alter the focal spot size to match the diameter of an imploding target. When implemented in the OMEGA system, these DPPs will greatly increase on-target energy efficiency in direct drive experiments.

The OMEGA's current focal spot diameter is unchanging during the beam pulse. Because of this, much of the energy misses the target after it shrinks from implosion. The newly modified DPPs have the ability to dynamically control the focal spot diameter on target to account for an imploding target. Simulated illumination shows that the new DPPs increase the late pulse percent intensity on-target from 27.5% to 73.4%. They also produce an azimuthally symmetric and super-Gaussian intensity profile to maintain reasonable irradiation uniformity.

2. INTRODUCTION

The distributed phase plate (DPP) is a full aperture diffractive element that serves to add phase to the laser beam incident upon the lens. An unaberrated beam passing through a perfect lens creates an Airy pattern (see ref. 1 p. 64) in the target plane, thus creating a focal spot diameter of 2 microns as opposed to the desired 1 mm target size. Any phase aberration present in the near field tends to spread the energy out of the perfect Airy pattern. The DPP is employed to modify the beam phase front and spread the energy over the entire target area. As in fig. 1, the incident light bypassing the DPP is focused onto an Airy pattern in the far field while the light passing through the DPP is spread about that point. Each section of the DPP is a different predetermined thickness of glass; this adds a controllable phase aberration to the beam. This beam, or near field, is then focused by the lens onto the target plane, or far field. The target field is located at the two-dimensional Fourier transform plane of the lens (see Ref. 1 pp. 83-90, Ref. 2); thus, the far field is the two-dimensional Fourier transform of the near field.
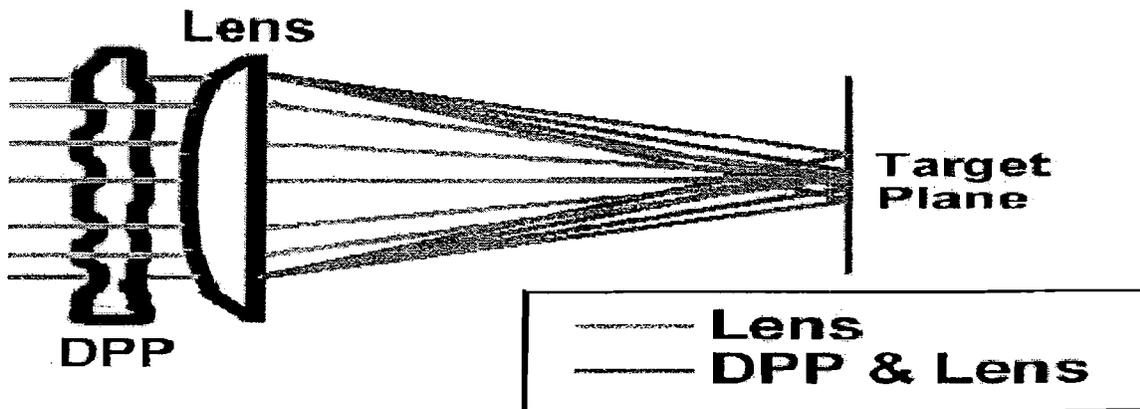

Fig. 1. Incident light bypassing the DPP is focused by the lens onto an Airy pattern of radius 2 microns in the target plane. Light passing through both the DPP and lens is diffracted about that point.

When the energy is spread out to many times the area of the Airy pattern, a speckle pattern forms as in fig. 2a. This speckle pattern is highly modulated due to the coherent interference in the far field. The process of smoothing by spectral dispersion (SSD) takes advantage of this high modulation. SSD spatially and temporally varies the beam phase such that the speckle pattern changes in time (see Ref. 3). As a result, the time-integrated far field has a smooth profile as in fig. 2b. These smoothed envelopes are those used in the DPP design process.

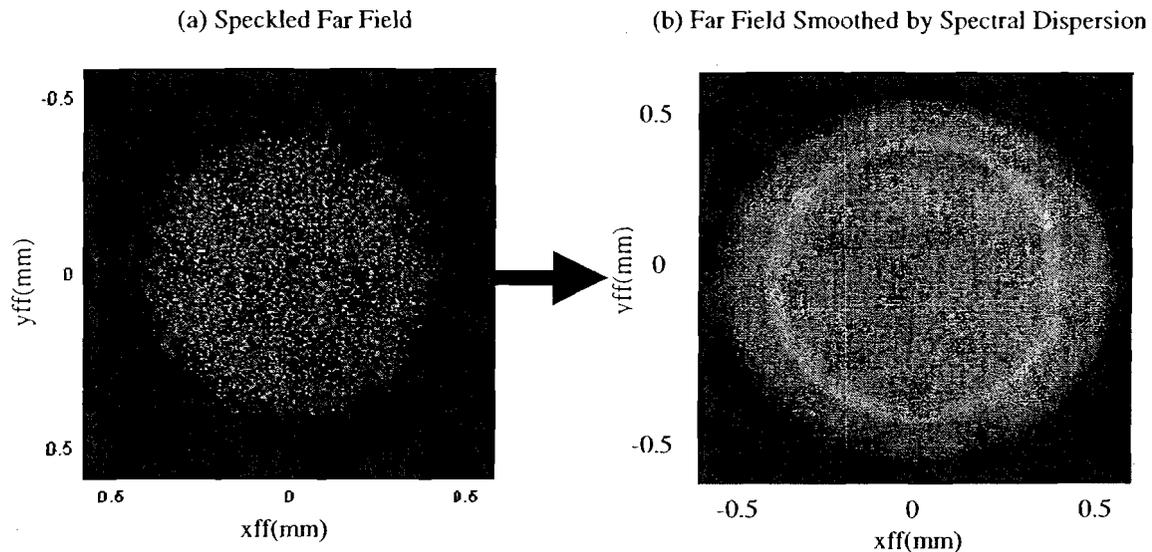(a) Speckled Far Field   (b) Far Field Smoothed by Spectral Dispersion

Fig. 2 Far field intensity images. The first is without Smoothing by Spectral Dispersion. The second is a time-integrated far field that has undergone smoothing by spectral dispersion.

The dynamic beam profile of the OMEGA laser system, in conjunction with the hybrid DPP, permits the far-field spot size to transform. Early in time, the intensity plot of the near field maintains a Gaussian profile as in Fig. 3a. As time progresses, the near field intensity plot transforms into an edge-peaked profile later in time as shown in Fig. 3b. In the Gaussian beam, a majority of the energy is concentrated in the center. In the

edge-peaked beam, the majority of energy is located at the outer edges. The DPP's ability to control the diffraction of the beam onto the far field is used to accomplish a dynamic spot size. Dividing the DPP into two corresponding regions permits control over two different regions in the far field. The inner disk region's radius is calculated by,

$$\pi r_d^2 = 0.5(\pi r_{DPP}^2),$$

$$r_d = \frac{1}{\sqrt{2}} r_{DPP},$$

where r_{DPP} is the radius of the DPP. The disk is used to control the far field early in time when it has a Gaussian profile. The annulus of the DPP, representing the remaining half, is used to control the far-field envelope later in time when the beam is edge-peaked. Thus, as the illumination of the DPP changes, so will the shape of the far-field envelope that it creates.

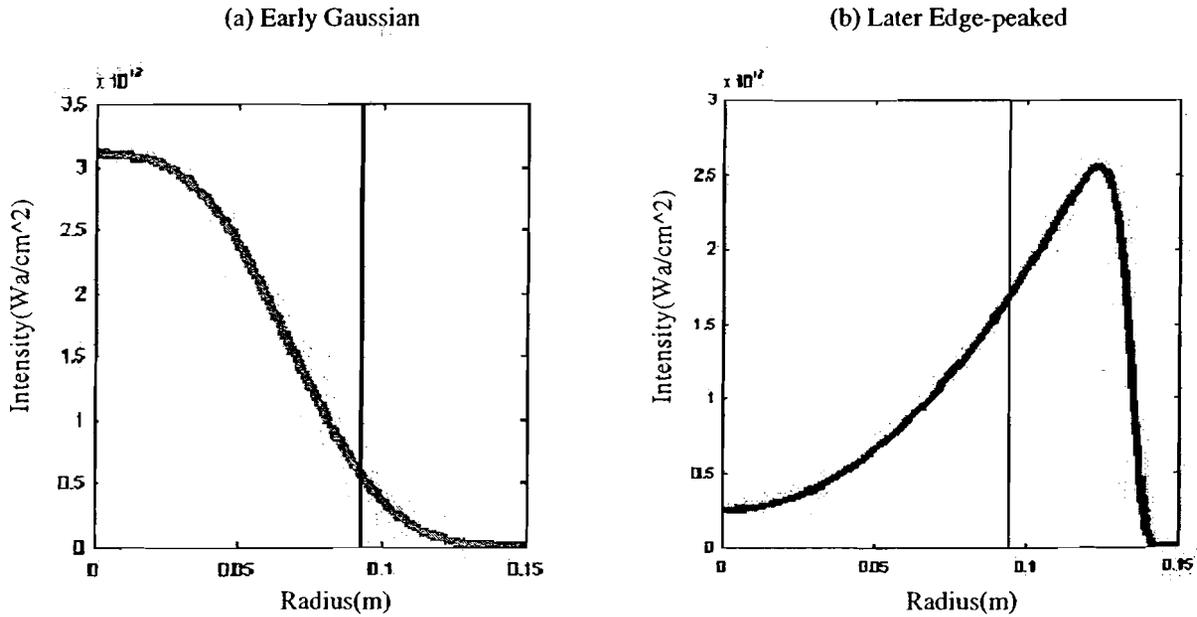(a) Early Gaussian   (b) Later Edge-peaked

Fig. 3 Near-field beam profiles that plot Intensity versus radius. The first is at a time of 0.8 ns and is Gaussian shaped while the second is at 2.8 ns and maintains an edge-peaked profile.

3. DYNAMIC FOCAL SPOT SIZE CONCEPT

The process of amplification undertaken in the Neodymium (Nd) glass rods modifies the OMEGA beam profile. Because the Nd rods are pumped externally using flash lamps, the outer region has more gain; therefore, the outside of the beam experiences increased gain during the pulse. Because the inside receives less energy from the pump rods, more energy is put through it to even the mid pulse energy profile. This results in a Gaussian beam profile early in time as in Fig. 3a. Once the flash bulbs pump the gain medium, the edges of the Nd glass rod are more able to produce gain; this causes the beam to be edge-peaked later in time as shown in Fig. 3b.

These anomalies of the amplification process provide a temporally varying quality that the newer DPP can exploit. In order to obtain a decreasing focal spot size, the DPP is divided into two separate regions, a disk and annulus of equal area. For simulation purposes, shooting for flat target super-Gaussian envelopes of high order is beneficial; as the super-Gaussian order increases, the smoother the beam intensity plot and more visible the aberrations. Early in time, before the target implodes, a desirable far-field envelope as in fig. 4a is given by,

$$I'_{ff} = e^{-\ln(2)\left(\frac{r}{r'}\right)^8},\tag{1}$$

where r is the radius and r′ is the peak-intensity half max. For the 1-mm target, the early r′ value is 0.6 mm. Since this far field is desirable early in time, the disk is modified to scatter energy as in equation 1. The desirable envelope for the imploded target is given by the equation,

$$I_{ff}'' = e^{-\ln(2)\left(\frac{r}{r'}\right)^8}.$$

(2)

Since the target has dramatically decreased in size, the r'' value is 0.2 mm. Modifying the annulus of the DPP to diffract energy as in equation 2 produces this smaller far-field envelope later in time.

(a) Early far field   (b) Later far field

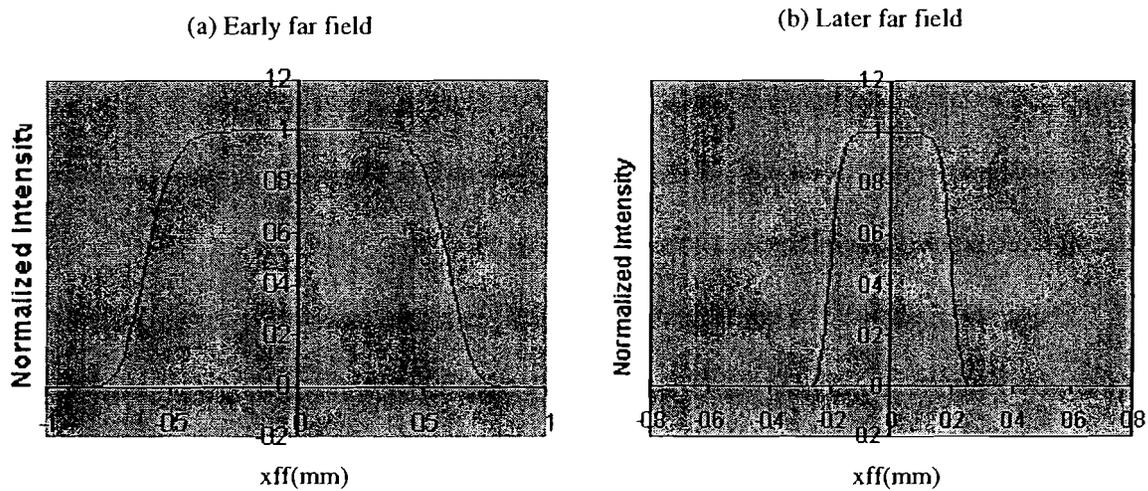xff(mm)   xff(mm)

Fig. 4. Two desirable far field envelopes of super-Gaussian order 8. The first is the early in time far field created by the disk of the DPP. The second is the later in time far field created by the annulus of the DPP.

4. SIMULATION AND CREATION OF THE MODIFIED DPP

Mathematical functions are used to model the near-field and far-field profiles on the OMEGA laser system. These functions are then manipulated by written code to perform DPP simulations as well as to create the DPPs. The data represented in fig. 3b may be modeled using a super-Gaussian function added to a polynomial function. Certain radii of interest are computed,

$$r_0 = r_p + 0.5d,$$
$$r_2 = r_p + d,$$

where r_p is the radius of the peak intensity value, r_0 is the radius of the location yielding 90% energy, r_2 is the radius yielding 10% energy and d is the radius differential from the intensity peak to the location yielding 10% of the intensity peak. Then, an initial guess at the polynomial coefficient is necessary. To determine the initial guess, assume that the super-Gaussian is near unity in the neighborhood of the peak value. Thus,

$$P = \frac{(I_p - y_i)}{r_p^2},$$

where P is the polynomial coefficient, I_p is the intensity value peak, and y_i is the y-intercept of the curve. Then, using the initial guess of the polynomial coefficient, an initial guess at the super-Gaussian order may be obtained,

$$m = \frac{\ln\{\frac{1}{\ln(2)}[\ln(y_i + Pr_2^2) - \ln(0.1I_p)]\}}{\ln(\frac{r_2}{r_0})},$$

where m represents the guessed super-Gaussian order. The super-Gaussian order may now be computed by solving the transcendental equation,

$$m' = \ln\left(\frac{1}{\ln(2)}\right)\left\{\ln\left\{y_i + \frac{\left[\frac{I_p}{e^{-\ln(2)(\frac{r_p}{r_0})^m}} - y_i\right]r_2^2}{r_p^2}\right\} - \ln(0.1I_p)\right\} - m\ln\left(\frac{r_2}{r_0}\right)$$

where m' is the actual super-Gaussian order. The actual polynomial coefficient, P', is calculated by,

$$P' = \frac{\left(\frac{I_p}{e^{-\ln(2)\left(\frac{r_p}{r_p}\right)^{m'}}} - y_i\right)}{r_p^2}$$

The equation for the edge-peaked near field intensity profile of fig. 3b is then given by,

$$I_{nf}^E = \sqrt{(y_i + P'r^2)e^{-\ln(2)\left(\frac{r_p}{r_0}\right)^{m'}}}$$ (3)

The equation for the Gaussian near field intensity profile of fig. 3a is modeled by,

$$I_{nf}^G = I_p e^{-\ln(2)\left(\frac{r}{ro}\right)^2},$$ (4)

where I_p is the peak intensity of the center of the Gaussian.

The phase of the DPP may be calculated from a given near field and a desired far field using an iterative process known as a Phase Retrieval Algorithm (see Ref. 4, 5, 6, 7). This algorithm uses two-dimensional spatial fast Fourier transforms to acquire the required near field for a given far field. Next, it determines the DPP phase necessary to convert the supplied near field into the necessary one. Because an exact DPP phase is not calculated on the first iteration, the loop is repeated with the new phase. The following iterations improve upon their predecessors until a reasonable accuracy is achieved. As a result, the Phase Retrieval Algorithm can be functionally expressed by,

$$\phi_{DPP}(x,y) = \Psi\{I_{nf}(x,y), I_{ff}(x_{ff},y_{ff})\}, \tag{5}$$

where ϕ is the DPP phase, Ψ is the Phase Retrieval Algorithm, I_{nf} is the given near field and I_{ff} is the desired far field.

The Phase Retrieval Algorithm is used in each step of a three-step process to create the DPPs. The first step creates a randomly initialized DPP that functions as a template for the individual regions of the DPP. This run assumes an early Gaussian beam profile and produces a full aperture DPP by,

$$\phi_{DPP}(x_{nf}, y_{nf}) = \Psi\{I_{nf}^G(x_{nf}, y_{nf}), I_{ff}^G(x_{ff}, y_{ff})\}, \tag{6}$$

from equations 1 and 4 decomposed into x and y components and equation 5 describing the Phase Retrieval Algorithm. The second step solely modifies the annulus of the DPP. The program is provided with the desired far-field envelope described in equation 2. Then, the program, instead of undergoing full aperture illumination in the iteration process, only illuminates the annulus by truncating the energy in the center region of the

beam. Once finished, the newly calculated annulus is cut and pasted onto the template

DPP from the original run. This process is represented by,

$$\phi_{DPP}(x'_{nf}, y'_{nf}) = \phi_{DPP}(x'', y'') + \Psi\{I^E_{nf}(x'_{nf}, y'_{nf}), I''_{ff}(x_{ff}, y_{ff})\}, \quad (7)$$

where x'_{nf} and y'_{nf} are the annulus's spatial components in the near field and x'' and y'' are

the disk-only components of the DPP phase generated from equation 6. The third step

only modifies the disk region of the DPP. As before, only this region of the DPP is

illuminated and the resulting phase data is placed on the template. This process is

represented by,

$$\phi_{DPP}(x''_{nf}, y''_{nf}) = \phi_{DPP}(x', y') + \Psi\{I^G_{nf}(x''_{nf}, y''_{nf}), I'_{ff}(x_{ff}, y_{ff})\}, \quad (8)$$

where x''_{nf} and y''_{nf} are the disk's spatial components in the near field and x' and y' are

the annulus-only components of the DPP phase generated in the process described in

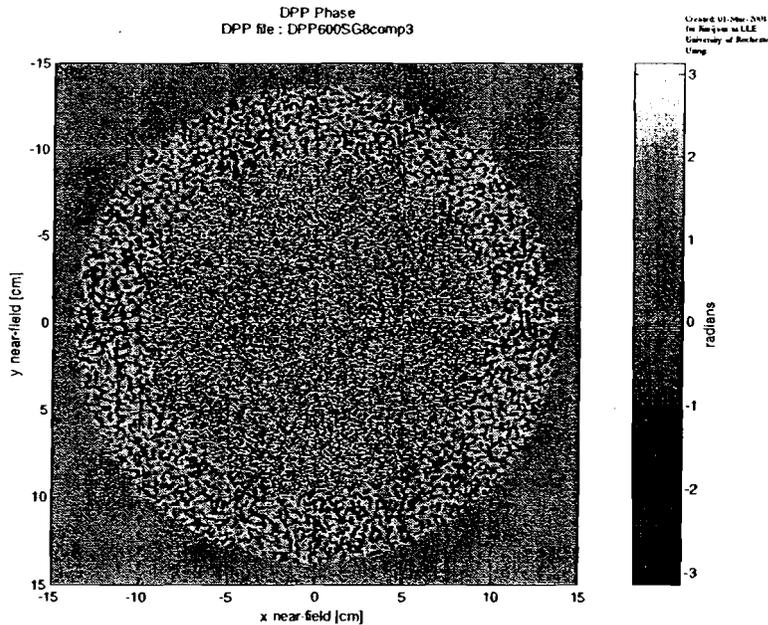equation 7. The output of this step is the newly modified DPP in fig. 5.

Fig. 5. DPP phase image and output of DPP creation program. Each gray shade represents a different thickness of the glass adding phase to the laser beam of pi to negative pi radians.

5. ACHIEVING HIGH IRRADIATION UNIFORMITY

The method of creating the DPPs solely involves illumination of each region individually. When the resultant DPP in fig. 5 is illuminated with a full aperture beam, energy found in the illumination overlap creates anomalies in the far field. Early in time, when a wide super-Gaussian envelope is desired, energy passing through the annulus creates a smaller super-Gaussian shaped bump in the far field as in fig. 6a. Later in time, a similar phenomenon occurs as energy passing through the disk creates a wide skirt in the far field as in fig. 6b. Although this causes an overall decrease in irradiation uniformity, the later example is inconsequential because it does not affect the irradiation uniformity on target. The early in time case, however, is a significant problem since it greatly distorts the desired far field envelope and will affect the stability of the imploding target.

(a) Early Profile   (b) Later Profile

Fig. 6 These illustrations describe the effect of energy in the illumination overlap. The dark gray energy has passed through the disk while the light gray energy has passed through the annulus.

Restoration of a desirable far-field envelope involves a method of compensation for the undesired energy due to the illumination overlap in the annulus. The target far field may be modified such that upon addition of the excess energy, the desirable far field

is obtained. Determination of the energy in the illumination overlap involves the integration of the equation representing the beam profile and then rotating it around the origin. Thus, total excess energy (U'), is given by,

$$U' = 2\pi \int_{r_d}^{r_{DPP}} \left[I_p I_{nf}^G \right] r \, dr, \tag{9}$$

where r_d is the radius of the disk and r_{DPP} is the radius of the whole DPP. Because this energy passes through the annulus of the DPP, it has the super-Gaussian far field shape that is created in that region. The equation representing the far-field bump is thus obtained by multiplying a normalized equation 2 by the excess energy found using equation 9,

$$I_b = \frac{U' I_{ff}''}{\int_0^\infty I_{ff}'' r \, dr}.$$

Compensating for this calculated energy simply involves subtracting this energy from the desired far-field envelope in equation 1,

$$I_{ff}' = I_{ff}' - I_b. \tag{10}$$

Then, as shown in fig. 7, illumination of the new DPP will allow the excess energy found in the illumination overlap to fill in the depression now present in the desired far field envelope of the disk. When the outcome of equation 10 is substituted for the far field from equation 1 in the DPP creation process, the result is the originally desired super-Gaussian far field and better irradiation uniformity.
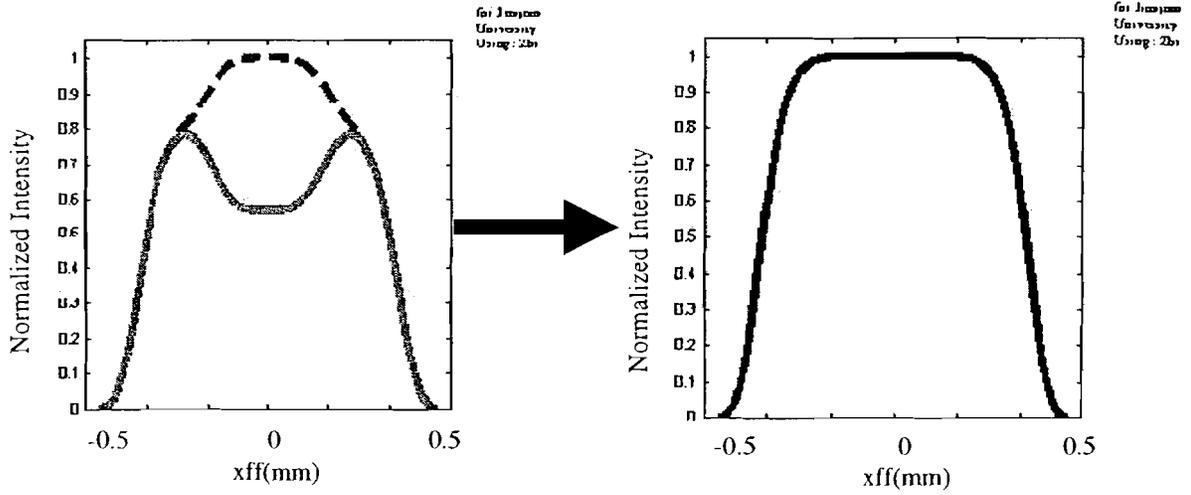
Fig. 7. The modified target far field produces a desirable far-field envelope by compensating for the illumination overlap in the annulus represented by the dotted line. The result is a desirable super-Gaussian far field.

6. TIME EVOLUTION OF THE FAR-FIELD ENVELOPE

In determination of the DPP phase data, two reference points were utilized, one describing the near-field profile at 0.8 nanoseconds and the other at 2.8 nanoseconds. In actuality, the jump between the two stages is not instantaneous, but gradual. And, as the near field changes in time, the far field temporally evolves. This section describes the procedure involved in determining the temporally evolving far-field envelope.

A model for the spatio-temporal evolution of the pulsed-beam on OMEGA is obtained by temporally blending the two reference near-field profiles. Using the blend function in fig. 8 and equations 1 and 2,

$$I_{nf}(x, y, t) = B_G(t)I_{nf}^G(x, y) + B_E(t)I_{nf}^E(x, y), \tag{11}$$

where B_G is the Gaussian component of the blend function and B_E is the edge-peaked component of the blend function. By illuminating the DPP with the full aperture, spatio-temporally evolving near field from equation 11, the evolving far-field envelope is obtained. This process is given by,

$$I_{ff}(x_{ff}, y_{ff}, t) = \left| \Im\{\sqrt{I_{nf}(x_{nf}, y_{nf}, t)}\} \right|^2, \tag{12}$$

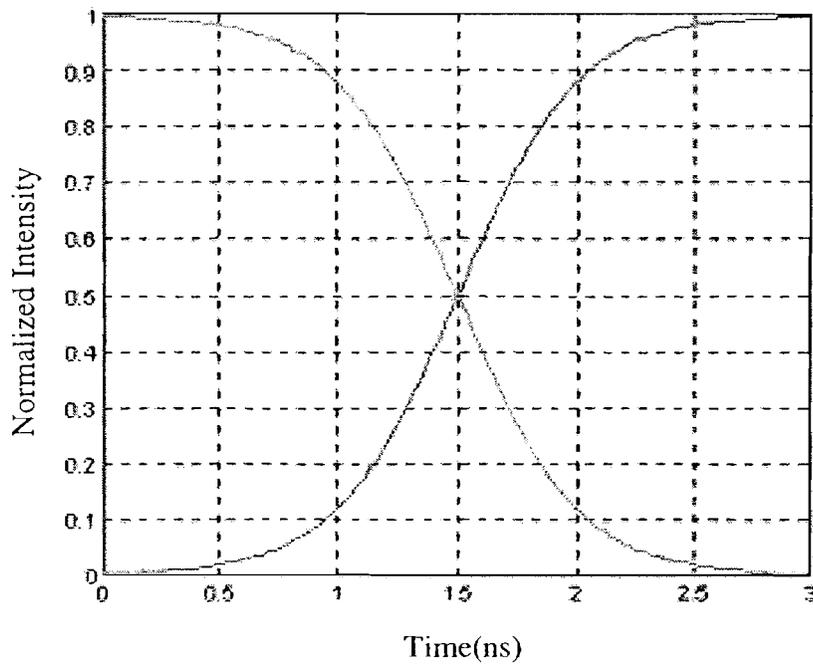where $\Im\{\}$ represents the spatial 2D Fourier transform.

Fig. 8. The Blend function used to add a temporal element to the near field. The light gray line is the magnitude of the Gaussian profile's influence while the dark gray line is the edge-peaked profile's power.

7. RESULTS

Upon illumination and simulation, several positive results are obtained. As shown in fig. 9, the far-field spot size decreases in size throughout the shot.
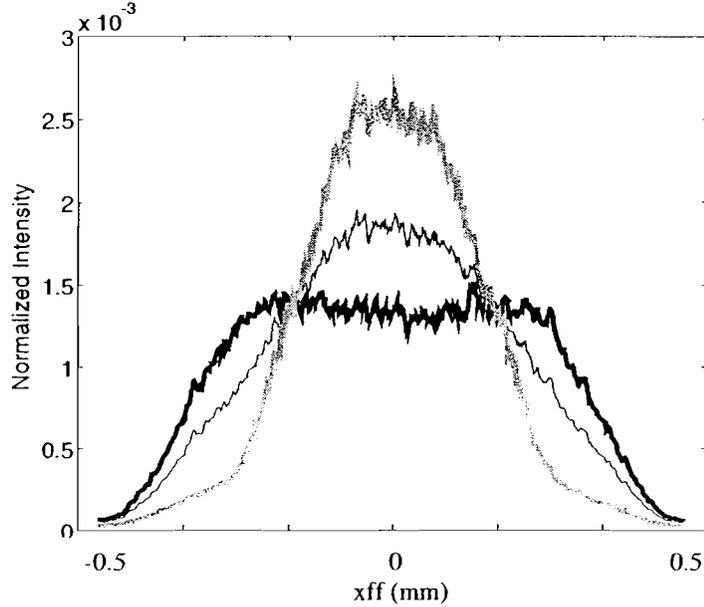

Fig. 9. Three Far-field lineouts. The thick, black line represents an early in time envelope, the thin black line is a mid-shot lineout and the gray line is extracted near the end of the 3ns shot.

In turn, the percent energy within the bounds of the imploded target also increases as shown in fig. 10. The energy ratio, $U_{\%}$, between energy on the small target and total energy is calculated at any time by,

$$U_{\%}(t) = \frac{\int_0^{.2} I_{ff}(t)rdr}{\int_0^{\infty} I_{ff}(t)rdr}.$$

The original DPP transfers 27.5% of the total energy onto the imploded target later in time. The modified DPP increases this to 73.4%, being over 2.6 times more efficient.
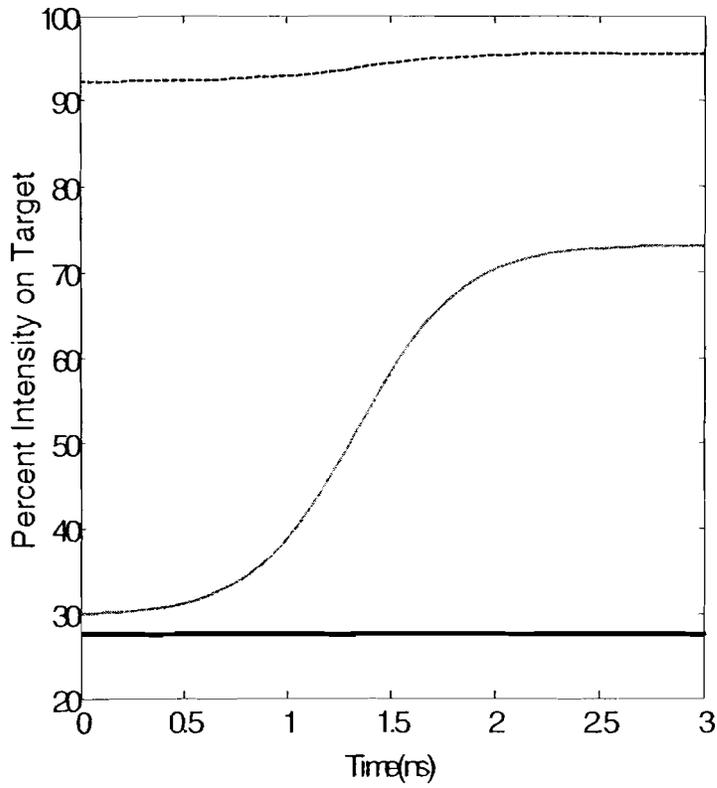
Fig. 10. This graph represents percent intensity on target over the 3ns shot. The dashed line depicts the percent energy in the modified DPP's far field that is transferred to the large, preimploded target. The thin gray line is the percent energy the modified DPP scatters onto the smaller, imploded target. The dark line is the percent energy that the original DPP transferred to the small target.

8. CONCLUSION

These new DPP's have demonstrated the ability to decrease the far-field spot size throughout the 3ns shot. They have also proven to maintain a high level of uniformity in the far-field envelope as well. The versatility of the DPP creation method provides added strength to the project. By altering variables, one can account for any size target, any given near field, and any desired far field. The hybrid DPPs already increase the OMEGA's late shot, on-target energy efficiency 2.6 times. If the current near-field profile could be better tailored using beam-shaping techniques, this could be increased as energy is eliminated from the illumination overlaps.

There is also interest in these modified DPPs being implemented in direct drive experiments to be performed on the National Ignition Facility in California. Instead of using cylindrical rods, the NIF employs slabs of gain medium that are more evenly pumped, thus eliminating many of the profile aberrations found in the OMEGA laser system. Further work could be done in attempt to determine if the current method could be altered to work on the NIF.

Fabrication of these modified DPPs requires additional manipulation of the DPP Phase data. The output of the DPP creation program is a matrix with varying phases at each point. Because a continuous relief is desired for the manufactured DPP, this data must be "unwrapped" such that instead of jumping from phase to phase, there is a continuous progression between neighboring phase values. Once "unwrapped", these DPPs can be fabricated and implemented in the OMEGA laser system, drastically increasing efficiency during direct drive experiments.

9. ACKNOWLEDGEMENTS

10. REFERENCES

1. J. W. Goodman, *Introduction to Fourier Optics* (McGraw-Hill, New York, 1968).

2. R.N. Bracewell, *The Fourier Transform and Its Applications,* 2nd ed., rev., McGraw-Hill Series in Electrical Engineering. Circuits and Systems (McGraw-Hill, New York, 1986).

3. S. Skupsky, R. W. Short, T. Kessler, R. S. Craxton, S. Letzring, and J. M. Soures, J. Appl. Phys. 66, 3456 (1989).

4. J. R. Fienup, "Phase retrieval algorithms: a comparison," *Appl. Opt.* 21(15), 2758-2769 (1982).

5. "Distributed-phase-plate design using simulated annealing algorithms," Laboratory for Laser Energetics LLE Review 64, NTIS document No. DOE/SF/19460-99, 1995 (unpublished), pp.170-174.

6. Y. Lin, T. J. Kessler, and G. N. Lawrence, "Design of continuous surface-relief phase plates by surface-based simulated annealing to achieve control of focal-plane irradiance," *Opt. Lett.* 21(20), 1703-1705 (1996).

7. Y. Lin, T. J. Kessler, and G. N. Lawrence, "Distributed phase plates for super-Gaussian focal-plane irradiance profiles," *Opt. Lett.* 20(7), 764-766 (1995).